Formation and Characterization of Chitosan Membranes

C. Clasen,* T. Wilhelms, and W.-M. Kulicke

Institute of Technical and Macromolecular Chemistry, University of Hamburg, 20146 Hamburg, Germany

Received May 18, 2006; Revised Manuscript Received August 7, 2006

In this paper, hydrophilic polymer membranes based on macromolecular chitosan networks have been synthesized and characterized. The structure of the membrane has been altered in several ways during the formation to adjust the properties, particularly with regard to the elasticity, tensile strength, permeability, and surface structure. An alteration of the network structure was achieved by addition of flexibilizer, cross-linking with dialdehydes, symplex formation of the chitosan with the polyanion sulfoethyl cellulose, and the introduction of artificial pores on the micro- and nanometer scale into the chitosan matrix with silica particles or poly(ethylene glycol). The resulting network structures and morphologies of these unique membranes that combine the novel alteration techniques have been characterized in detail and correlated with molecular parameters of the chitosan as degree of deacetylation, molar mass, and charge density. Finally, we report on the impact of the new network structures on physical properties of the membranes, the water vapor and gas permeability and the tensile strength, to evaluate possible application of the membranes as a wet wound dressing material with microbial barrier function that actively assists the healing process of problematic wounds. Parts of the novel combined membrane alteration and formation techniques are now covered by the patent DE 102004047115.

1. Introduction

Hydrophilic polymeric membranes have in general a high swellability, high permeability for water vapor and gases, good fluid transport via the membrane, and a high selectivity for the transport of voluminous and apolar substances. These properties in combination with an adequate mechanical strength make them highly desirable for the treatment of wounds as a coverage material. As was already mapped out by Winter in 1962[1] and later rephrased by Turner,[2,3] modern wound dressings require a moist climate with sufficient fluid transport from and a gas transport to the wound across the membrane to ensure an aerobe climate while at the same time providing a barrier function against infections and thermal isolation. The exact tailoring of the polymers and their three-dimensional structure to achieve these properties of a moist wound dressings is of utmost importance, because synergic effects of the transport phenomena may lead to undesired substance accumulation.[4]

To date, there are already several moist wound dressings commercially available, most of them based on a synthetic polyurethane carrier matrix in combination with an embedded hydrogel (agar, gelatine, or carboxymethyl cellulose) or as a simple gel based on concentrated carboxymethyl cellulose gum, Ca-alginates, or collagen matrixes.[5] However, especially for the treatment of problematic wounds such as burns and chronic wounds, the commercially available wet wound dressings are insufficient. Chronic wounds caused 2 million lost working days per year in Germany alone (according to the compulsory health insurance funds, Germany, 2001), and burns require an atraumatic wound dressing that can easily be removed because these wounds are especially sensitive to a retraumatization and have a high degree of wound pain.[6] These problematic wounds also require not just a purely physical wound coverage, but an additional stimulation to support the healing process.

Recently, a new type of wet wound dressing membrane based on chitosan has been introduced[7] that is applicable for the treatment of problematic wounds. Chitosan membranes have been commercially available as HemCon since 2003 (HemCon, Portland, OR) and Chitoskin (SanguiBioTech GmbH, Witten, Germany) since 2004.

The advantage of chitosan as a material for wet membranes in comparison to polyurethane-based membranes is the high water permeability and the ability to immobilize microorganisms.[8,9] Chitosan may also accelerate wound-healing,[10−13] has haemostatic properties and stimulates macrophage activity,[14] has been reported to inhibit the growth of tumor cells,[15] and shows a general antimicrobial effect.[16−19]

However, so far there are no fundamental investigations of the fluid and gas permeability and the causal membrane parameters for chitosan. An understanding of how these material properties can be properly adjusted is highly desirable because the amount of wound exudate can vary from large quantities for burns to relatively dry conditions in chronic wounds. To achieve the optimal wet wound climate, the wound dressing and its fluid and gas transport capabilities need to be tailored to the specific conditions. This requires an effective understanding of the membrane structure to enable the adjustment of the desired permeability, barrier function, and thermal isolation of a wound while maintaining a mechanically stable membrane.

We therefore present in this paper investigations on the formation and alteration of chitosan membranes by several physical and chemical processes such as cross-linking, symplex formation, introduction of macro- and microporosity, and reinforcing. We show how the resulting morphological changes in the network parameters, pore size distribution, and surface structure lead to improved properties as gas and fluid permeability, elasticity, ductility, and tack. Parts of the new formation and alteration techniques are covered by a patent.[20]

The paper is structured as follows: the first part of the discussion deals with several novel alteration methods of chitosan membranes and discusses in detail the structural and property bandwidth achievable with the single methods. The second part then compares representative membranes of the single alteration techniques as well as novel membranes that combine the different alteration techniques to create up to now

10.1021/bm060486x CCC: $33.50
Published on Web 09/28/2006

Table 1. Molecular Parameters of the utilized Chitosan Samples

chitosan sample	$[\eta]$/(mL/g)	M_w/(kg/mol)	DDA (degree of deacetylation)
A	578	253	0.84
B	685	318	0.79
C	1007	587	0.75
D	524	221	0.98
E	719	340	0.86

unequaled permeabilities and mechanical strengths and evaluates their application properties as moist wound dressings.

2. Experiments and Methods

2.1. Sample Characterization. *2.1.1. Chitosan.* Chitosan was provided by Biomex GmbH (Mannheim, Germany), Cognis Deutschland GmbH & Co. KG (Düsseldorf, Germany), Fluka (Buchs, Switzerland), SeeLab (Wesselbürenkoog, Germany), and Sigma-Aldrich (Seelze, Germany) and the Department of Biotechnology of Kaliningrad State Technical University (Russia). All chitosan samples investigated in this paper were isolated from crustaceans. The samples contained up to 0.9 wt % insoluble constituents that were separated by filtration during the solution preparation. The molar mass M_w of selected chitosan samples was determined from intrinsic viscosities via the Mark−Houwink−Sakurada relationship $[\eta]/(g/mL) = 5.80 \times 10^{-2}(M_w/(g/mol))^{0.74}$.[21] Intrinsic viscosities were determined from aqueous solutions, containing 0.5 mol/L acetic acid and 0.2 mol/L sodium acetate, with an Ubbelohde capillary viscometer utilizing a Ic capillary (Schott GmbH, Mainz, Germany).[22] The average degree of deacetylation (DDA) of the chitosan, describing the ratio of 2-aminodesoxy groups to the overall number of glucose units in a polymer molecule, was determined via ^{13}C NMR and ^{1}H NMR spectroscopy of the chitosan samples, ultrasonically degraded for a better resolution of the spectra.[22] The NMR spectroscopic investigation of the soluble parts of the samples revealed no impurities from residual proteins. The polymer analytical results for the different chitosan samples are given in Table 1.

2.1.2. Sulfoethyl Cellulose. The sulfoethyl cellulose (SEC) samples were provided by Wolff Cellulosics (Walsrode, Germany). The molar mass M_w of the SEC samples was determined from intrinsic viscosities in 0.1 M sodium nitrate solution via the Mark−Houwink−Sakurada relationship $[\eta]/(g/mL) = 4.28 \times 10^{-3}(M_w/(g/mol))^{0.95}$.[21] The average degree of substitution (DS) of the SEC, describing the ratio of sulfoethyl groups to the overall number of glucose units in a polymer molecule, as well as the regiospecific degree of substitution (RS), describing the ratio of sulfoethyl groups at a specific position of the glucose to the overall number of glucose units, was determined via ^{13}C NMR spectroscopy of the SEC samples, ultrasonically degraded for a better resolution of the spectra. The polymer analytical results for the different SEC samples are given in Table 2.

2.2. Membrane Formation. *2.2.1. Chitosan Membrane Formation.* Chitosan (3 wt %) was dissolved in 1 wt % acetic acid by stirring for at least 3 h. The solution was then filtered with a 330 μm steel mesh to separate possible insoluble particles. A film (2 mm) of the solution was applied to a flat polycarbonate surface and dried at 60 °C for 12 h.

2.2.2. Chitosan Membrane with Flexibilizer Glycerol. A defined amount of glycerol (0.5−3 wt %) was added to the acetous (1 wt % acetic acid) chitosan solution (3 wt %). This glycerol amount is equivalent to 16−100% of the amount of chitosan in the solution. The solution was stirred for several minutes, and a film (2 mm) of the solution was applied to a flat polycarbonate surface and dried at 60 °C for 12 h.

2.2.3. Partially Cross-Linked Chitosan Membranes. Three grams of chitosan was dissolved in 97 g of a 0.75 wt % solution of acetic acid and cooled to 4 °C. To this solution was added 20 g of a cooled solution of the respective amount of the cross-linker glyoxal or glutaraldehyde (0.6, 0.3, 0.15, and 0.05 g) dissolved in 0.75 wt % acetic acid. The mixed solutions were immediately homogenized by vigorous stirring for 2 min. A thin film (2 mm) of the solution was applied to a flat polycarbonate surface and dried at 60 °C for 12 h.

2.2.4. Macroporous Chitosan Membrane Formation. A defined amount of silica particles (6 wt %) with a nominal diameter range of 40−63 μm was added to an acetous (1 wt % acetic acid) chitosan solution (3 wt %). A film (2 mm) of the solution was applied to a flat polycarbonate surface and dried at 60 °C for 12 h. The membrane was then placed in an aqueous solution of sodium hydroxide (8 wt %, Merck KGaA, Darmstadt, Germany) for 2 h at 60 °C to dissolve the silica particles. The membrane was then rinsed with water and dried at 60 °C for 6 h.

2.2.5. Microporous Chitosan Membrane Formation. A defined amount of poly(ethylene glycol) (6 wt %) (PEG, Merck KGaA, Darmstadt, Germany) with a molar mass of 35.000 g/mol was added to an acetous (1 wt % acetic acid) chitosan solution (3 wt %). A cellulose mesh (filter paper with a thickness of ∼120 μm) was completely soaked in the solution, placed on a flat glass surface, and coated with a 4-mm thick film of the chitosan/PEG solution. The membrane was dried at 60 °C for 12 h. The dried membrane was then immersed in a 0.5 wt % sodium hydroxide solution (Merck KGaA, Darmstadt, Germany) for 24 h to dissolve the PEG and then rinsed with water to pH = 7.

2.2.6. Chitosan−Sulfoethyl Cellulose Symplex Membrane Formation. A thin film (0.25 mm) of 3 wt % aqueous solution of sulfoethyl cellulose was applied to a flat glass surface. The SEC film was then dipped into a solution of 0.5 wt % chitosan dissolved in 0.5 wt % acetic acid for 30 min. The developed membrane was then rinsed with water, transferred to a polyethylene foil, and dried at room temperature.

Reinforced chitosan symplex membranes were synthesized by dipping a cellulose mesh (gauze bandage, Lohmann & Rauscher GmbH & Co. KG, Neuwied, Germany) into a 3 wt % aqueous solution of sulfoethyl cellulose. The mesh was then immersed in a solution of 0.5 wt % chitosan dissolved in 0.5 wt % acetic acid for 60 min. The developed reinforced symplex membrane was then rinsed with water and dried at room temperature.

2.3. Polymer and Membrane Characterization. *2.3.1. NMR Spectroscopy.* The IGATED ^{13}C spectra and ^{1}H spectra of the Chitosan and SEC sample were obtained with a Bruker Avance 400 spectrometer (Rheinstetten, Germany) and evaluated with ACD Lab SpecView (Bremen, Germany).

2.3.2. Scanning Electron Microscopy (SEM). Scanning electron microscopy pictures of the samples were obtained with a Hitachi S-4800 field emission SEM (Hitachi High-Technologies Europe GmbH). A cryofixation of the wet and swollen membranes was achieved by shock-frosting the samples in liquid nitrogen and the subsequent removal of the solvent by freeze-drying at −70 °C under high vacuum. The samples

Table 2. Molecular Parameters of the utilized Sulfoethyl Cellulose (SEC) Samples (DS = Average Degree of Substitution, RS = Regiospecific Degree of Substitution)

SEC	$[\eta]$/(mL/g)	M_w/(kg/mol)	DS	RS at C2	RS at C3	RS at C6
1	582	253	0.51	0.08	0.16	0.27
2	608	266	0.34	0.04	0.07	0.23
3	419	180	0.36	0.07	0.11	0.18
4	432	186	0.40	0.07	0.11	0.22
5	530	230	0.40	0.06	0.11	0.23

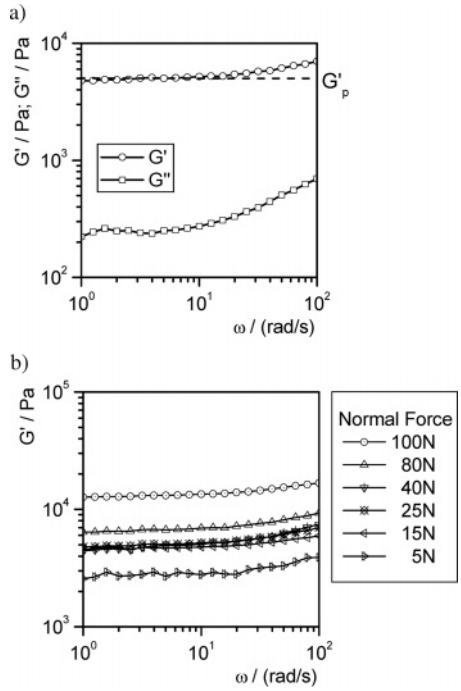

Figure 1. (a) Storage and loss modulus G' and G'' as a function of the applied frequency ω for a wet chitosan membrane with an applied normal force of 25 N. The frequency-independent region of the storage modulus G' allows the determination of the plateau modulus G_p'. (b) Storage moduli for the same sample at different levels of normal force.

were sputtered with a 10 nm gold layer to ensure a thorough coverage of the highly porous samples.

2.3.3. Confocal Microscopy. Confocal microscopic images have been taken with a Leica TSC SP2 (Leica Microsystems Mannheim GmbH, Mannheim, Germany). The membrane samples were soaked in water prior to the microscopic investigation and swollen to an equilibrium state.

2.3.4. Rheological Oscillatory Measurements. The rheology of the membranes in dynamic shear flow for the determination of the storage modulus G' and loss modulus G'' was investigated using a TA Instruments Rheometric Series ARES rheometer (TA Instruments, Newcastle, DE) with plate-and-plate fixtures ($Ø = 50$ mm). All moduli were measured in the experimentally determined linear-viscoelastic limit of deformations of 0.5−1.9%. The plateau modulus G_p' was determined from the frequency-independent regime of the storage modulus G' as indicated in Figure 1a.

To ensure a continuous contact of the not completely even surface of the chitosan membrane to the surfaces of the fixtures, a normal force of 25−30 N was applied. The used normal forces lie in the applicable regime of normal forces that do not influence the measured moduli, determined by a series of frequency sweeps at increasing normal forces as shown exemplarily in Figure 1b. Too high normal forces (in the shown case >40 N) result in an increasing plateau modulus due to deformation of the network structure, and too low normal forces (<15 N) do not ensure a sufficient contact of the fixture to the membrane surface and result in a decreasing plateau modulus. For chitosan symplex membranes, the applicable normal force level was determined to be lower (~5 N).

2.3.5. Rheological Stress−Strain Measurements. The stress−strain behavior of the membranes was tested on a Z010 material tester (Zwick/Roell, Ulm, Germany). The test samples were cut from the membranes to a length of 50 mm and a width of 4.1 mm. The strain along the length of the sample was increased with a velocity of 0.1 mm/s.

2.3.6. Gas Permeation. The gas permeability of the membranes was tested with a custom built pressure-gradient apparatus (GKSS, Geesthacht, Germany), which allows the determination of the gas flux at discrete pressure gradients across the membrane. The pressure gradient

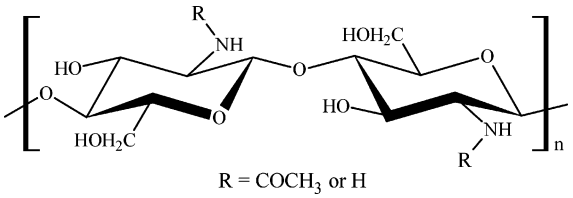

Figure 2. Structure of chitin or chitosan. Chitosan is characterized by a high degree of deacetylation (DDA) at the nitrogen.

was stepwise increased with time until steady flux conditions were reached. The apparatus allowed the testing of permeabilities for different gases (H_2, O_2, CO_2, and N_2) in a single run.

2.3.7. Water Vapor Permeation. In cases where pressure gradient gas permeability measurements could not be performed on a membrane, for example, in a wet state or when swollen with higher amounts of glycerol, the permeability of the membrane can be tested with water vapor permeability measurements.

The water vapor permeability of the membranes was determined from a comparison of the water vapor flux from a saturated atmosphere with a relative humidity of 75% at 25 °C via the membrane to a completely dry atmosphere. The relative water vapor permeability of these membranes was defined as the amount of water transferred from a saturated to a dry atmosphere with no membrane as compared to the vapor transferred through the respective membrane. The amount of water per time and area was recorded by weight.

2.3.8. Porosimetry. The pore size distribution was determined with a mercury Porosimeter 2000 (Carlo Erba Instruments, Milano, Italy). The average contact angle of mercury/chitosan systems was determined to be 141.3°.

3. Results and Discussion

3.1. Chitosan Membranes. Chitosan is a copolymer consisting of randomly distributed β-(1-4)-linked D-glucosamine and *N*-acetyl-D-glucosamine (Figure 2) and is commercially produced by deacetylation of chitin from the exoskeleton of crustaceans. The degree of deacetylation (DDA) determines the solubility of chitosan in acidic solution and the ability to re-form supramolecular structures via hydrogen bonding after evaporation of the solvent.

The ability of chitosan to form membranes by a simple solvent evaporation from a low concentrated organic acid and subsequent neutralization has already been investigated in the past[23,24] (for a recent overview of several known methods to produce membranes from chitosan, see ref 14). Therefore, various applications for this kind of membrane have recently evolved. The immobilization ability of chitosan membranes makes it a useful carrier material for biosensors;[25,26] chitosan is also discussed as a scaffold for tissue engineering[27,28] and has proven to be a strong metal ion binder.[29,30] Chitosan membranes are under investigation for selective separation in fuel cells,[31] dehydration of ethanol,[32] and as carrier material for ferrimagnetic membranes.[33]

However, pure chitosan membranes have severe disadvantages for the usage as wet wound dressings. Even though chitosan accelerates wound-healing,[10,11] has haemostatic properties, and shows a general antimicrobial effect,[16−19] the membranes formed from solely chitosan show an insufficient permeability for wound exudate and are not flexible enough in a dry state to allow proper handling during the application process. To improve those disadvantages, the swelling grade of a chitosan membrane with a permeable but involatile solvent[34] can be utilized to optimize the mesh width and therefore the permeability of the amorphous membrane.[35]

3.1.1. Swelling of Chitosan Membranes with Glycerol. The presence of glycerol during the membrane formation process

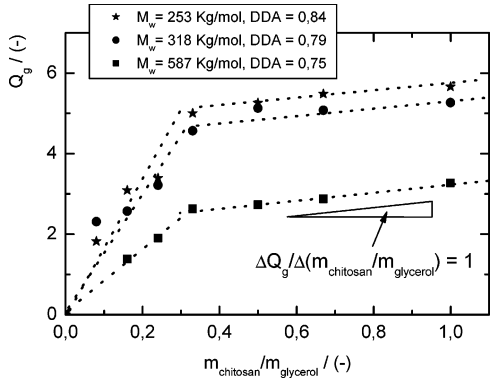

Figure 3. Swelling ratio Q_g for different chitosan membranes depending on the glycerol content.

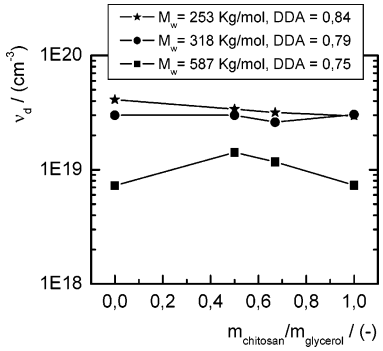

Figure 4. Reduced netpoint density ν_d of membranes from different chitosan samples and for different glycerol contents.

leads, after the removal of the solvent water in the subsequent drying process, to a swollen membrane that shows improved flexibility and permeability. However, the hydrophilic glycerol always entraps additional water in the membrane even in a "dried" state. Because it is not possible to completely remove the glycerol from the membrane, the determination of the actual mass of the dry, glycerol-free membrane is not directly accessible. To determine the actual swelling of the glycerol membranes, we therefore used a recursive method. For this, we determined the complete swelling ratio $Q_{H_2O} = V_{H_2O}/V_g$ of the glycerol membrane in an excess of water (with V_g as the volume of the dry glycerol membrane and V_{H_2O} as the volume of the completely swollen membrane) and the complete swelling ratio $Q_0 = V_{H_2O}/V_d$ of the glycerol-free membrane (with V_d as the volume of the dry, glycerol-free membrane) in an excess of water. We then obtain the true swelling of the membrane solely from the glycerol from:

$$Q_g = \frac{Q_0}{Q_{H_2O}} = \frac{V_g}{V_d} \tag{1}$$

A justification of this method, especially the question if the complete swelling and washing of the glycerol containing membranes will lead to the same maximum swelling grade regardless of the initial glycerol content, is given by the oscillatory measurements of the completely swollen membranes. A comparison of completely swollen membranes with different initial glycerol contents gave the same plateau moduli G_p' for all membranes and therefore the same degree of swelling.

Figure 3 shows the dependency of the swelling from the amount of entrapped glycerol for different molar masses and DDA (degree of deacetylation). Obviously, for all chitosan samples an additional swelling due to entrapped water is observed up to a chitosan/glycerol ratio of ~0.35, indicated by the slope of the curves >1. A synergetic effect of the membrane and glycerol at these low glycerol concentrations causes this additional water to be strongly adhered to the network structure and immobilized so that evaporation during the normal drying process is prohibited. Above this critical value, the increasing swelling can be attributed solely to the increasing glycerol content as indicated by the slope of 1 in Figure 3. Even though a direct compatibility of the different chitosan samples is not possible because they vary in two parameters, the molar mass and the DDA, it seems that an increasing molar mass and a decreasing DDA lead to a less glycerol swellable network.

A determination of the network parameters of the swollen network is possible via the plateau region of the storage modulus G' from the small amplitude oscillatory shear experiment (i.e., the plateau modulus G_p'). In this frequency range, the induced energy is stored elastically by the polymer strand between two entanglement or network points, acting as an entropic spring. Therefore, the number density ν of these structural elements can directly be calculated from the measured plateau modulus[36] by the simple relation:

$$G_p' = \nu k_B T \tag{2}$$

where k_B is the Boltzmann constant. However, because the swelling of the network leads to an increasing distance between netpoints, a comparison of the network structure for different swelling states is only feasible for a reduced netpoint density

$$\nu_d = \nu Q = \frac{G_p' Q}{k_B T} \tag{3}$$

which gives the netpoint density for an unswollen state with Q as the prior determined swelling ratio Q_g for the glycerol membranes or the swelling ratio Q_0 for completely swollen membranes in water. It can clearly be seen that the reduced netpoint density for the different chitosan samples correlates with the swellability in Figure 4. The lower the netpoint density and therefore the lower the number density of meshes, the lower is the swellability.

Also, one can see in Figure 4 that the reduced netpoint density ν_d is independent of the glycerol concentration and also does not change even for a fully swollen state. Therefore, the addition of glycerol does not change the length of the polymer chain between two entanglement points; it only increases the widths of the network meshes by swelling them but does not influence the primary network formation in the wet state at which the glycerol is already present. The results also show that the netpoints of the chitosan network are stable in aqueous solution, a condition that is not trivial because the chitosan does not form chemical cross-links but rather forms netpoints through intermolecular interactions via hydrogen bonding.[37]

The increasing mesh width with rising glycerol content, however, does influence the permeability of the membrane. Simple chitosan membranes are reported to have a moderate permeability for water vapor.[38] The relative water vapor permeability of these membranes, defined as the amount of water transferred from a saturated to a dry atmosphere with no membrane as compared to the vapor transferred through the respective membrane,

$$L_{r,H_2O} = \frac{m_{H_2O,membrane}/t}{m_{H_2O}/t} \tag{4}$$

is shown in Figure 5. As one can see, below a critical glycerol

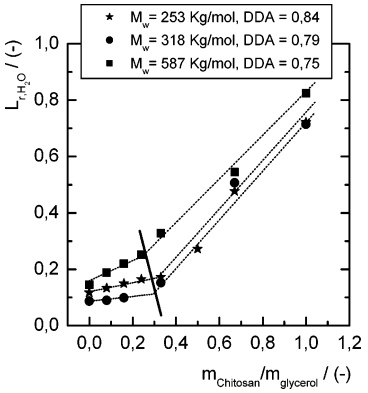

Figure 5. Relative water vapor permeability L_{r,H_2O} of membranes from different chitosan samples and for different glycerol contents.

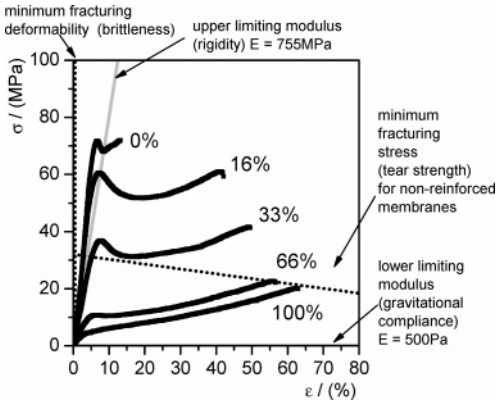

Figure 6. Stress σ as a function of the applied strain ϵ for chitosan membranes with different glycerol contents. In addition, different critical stress and strain limits for the applicability of membranes as wet wound dressings are given.

concentration, the permeability of water is slightly increasing with the glycerol concentration. The slope as well as the level of the curves below this critical glycerol concentration seem to be associated with the glycerol swellability in Figure 3; the less swellable, the more permeable the membranes are to water. Above the critical glycerol concentration in Figure 3, the permeability shows a much stronger increase with an increasing glycerol content of the membrane. The water permeability rises from a moderate level to ~80% at a ratio $m_{\text{chitosan}}/m_{\text{glycerol}} \approx 1$, the upper limit of glycerol concentration in the present study. The critical glycerol concentration of this onset of vast increase of permeability is again in accordance with the critical concentration of water immobilization in Figure 3. Below this critical concentration, the water immobilizing effect of the membrane observed in Figure 3 also hinders the permeability, resulting in the moderate and only slowly increasing water permeability in Figure 5.

The increasing glycerol content also influences the mechanical stability of the membranes, which can be determined from the stress response of the membrane to an applied strain (stress−strain tests). As shown in Figure 6, an increasing glycerol content lowers the Young's modulus

$$E = \frac{\sigma}{\epsilon} \tag{5}$$

of the membrane, observable as the initial slope of the curves in Figure 6. Here, σ is the stress and ϵ is the strain or deformation. The Young's modulus as a measure for the stiffness is a key criterion for the applicability of a membrane. Therefore, Figure 6 also gives a critical Young's modulus (upper limiting modulus) of $E = 755$ MPa, above which the rigidity of the membrane prohibits the practical applicability.

It has to be noted that the value of this critical Young's modulus is purely empirical and determined from the hands-on experience in our lab of applying membranes of a standard average cross-section area of ~10 mm^2 to human skin of the upper arm. However, this empirical value is very useful in estimating the applicability of new membranes. As can be seen in Figure 6, the addition of at least 33% glycerol during the formation of the membrane leads for this chitosan to Young's moduli below this critical maximum value. At the same time, the maximum deformability of the membranes increases and allows for an even better handling.

A lower limit of the Young's modulus E for the application of the membrane is given by a possible gravitational sagging of the membrane, when the softness of the membrane leads to unbearable deformations of unsupported parts of the membrane during application. A rough estimate of this modulus is given by

$$E = \rho g k \tag{6}$$

with ρ as the density, g as the gravitational constant, and k as a characteristic length scale, defining the ratio of sagging depth to unsupported length of the membrane. Again, the determination of a practical empirical value for this length scale from our practical application experience of membranes to human skin gives $k = 0.05$ m and therefore a Young's modulus of $E \approx 500$ Pa for a membrane of a standard average cross-section area of ~10 mm^2. As indicated in Figure 6, this lower limiting Young's modulus (lower limiting modulus or gravitational compliance) is far below the observed values for the chitosan membranes.

Another critical parameter of the mechanical strength is the minimum stress level a membrane has to sustain during application (minimum fracturing stress or tear strength in Figure 6). Even though the rupture stress in a purely elongational deformation, as exerted in this experiment, does not give the stability of a membrane against punctual rupture (due to inhomogeneous deformation processes as they mainly occur during the application), it can roughly be correlated with this stress value.[39] Again, an empirical value for this value has been obtained from hands-on experience of membrane application shown as the dotted line in Figure 6. This minimum stress value, which the membrane has to sustain, decreases with an increasing deformation, because larger deformations are easier to avoid if a critical stress level is exerted in the manual manipulation of the membrane. As can be seen in Figure 6, an increasing glycerol content generally decreases this critical level, which refers to the endpoint of the experimental curves in Figure 6. The chitosan membranes with glycerol contents larger than ~50% already have rupture stresses close to this limiting line and have therefore to be handled with greater care, diminishing their applicability. It should be noted that the occurrence of an ϵ-rupture, as observed in the maximum/overshoot of the stress strain curves for low glycerol contents, already marks the critical deformation for a rupture in manual manipulation of the membrane, because it is generally not possible to control the deformation fast enough after the stress level of the ϵ-rupture is overcome, to avoid the rupture at the final deformability limit.

A minimum fracturing deformability or brittleness limit, as indicated in Figure 6, is generally not important for the investigated systems. All chitosan-based membranes are flexible enough, even in the absence of glycerol, to exceed this minimum deformability limit (below which a bending deformation leads

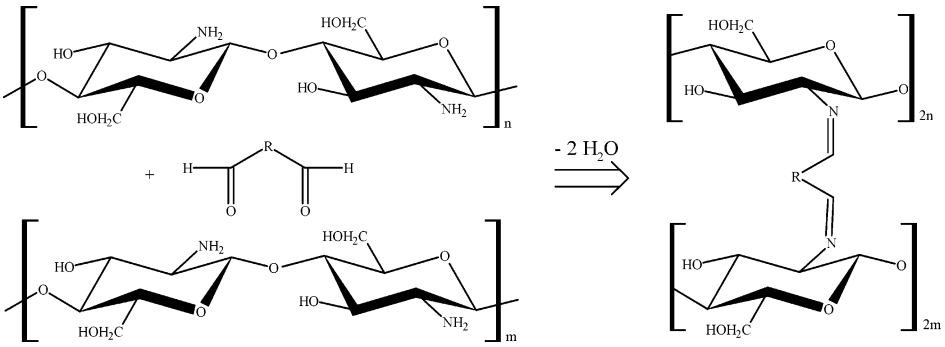

Figure 7. Cross-linking reaction of chitosan polymers via free amino group and dialdehydes.

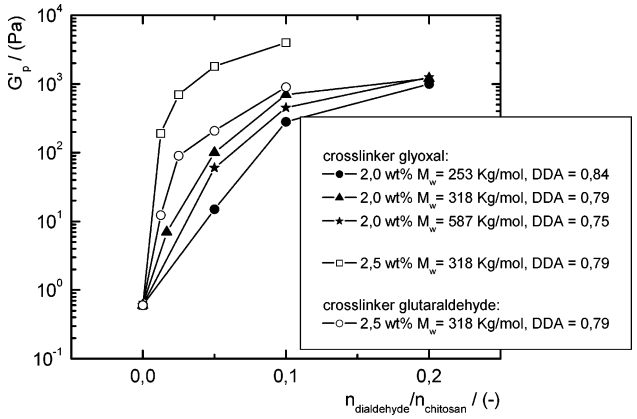

Figure 8. Plateau modulus G_p' as a measure for the netpoint density for different molar number ratios of cross-linking dialdehyde ($n_{dialdehyde}$) and chitosan monomers ($n_{chitosan}$).

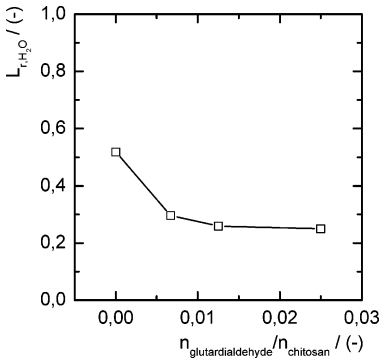

Figure 9. Relative water vapor permeability L_{r,H_2O} of cross-linked chitosan (M_w = 318 kg/mol, DDA (degree of deacetylation) = 0.79) membranes as a function of the molar number ratio of cross-linking glutaraldehyde ($n_{glutaraldehyde}$) and chitosan monomers ($n_{chitosan}$).

to a breaking of the membrane) and to rupture not until orders of magnitudes larger deformations are reached.

It should generally be noted that chitosan membranes investigated in this report with an average thickness of ~100 μm could be synthesized to larger thicknesses to increase the mechanical strength; however, this has to be evaluated versus the decreasing permeability.

3.1.2. Chemically Cross-Linked Chitosan. An additional chemical cross-linking of chitosan[40,41] with dialdehydes[32] or epoxids[42,43] leads to denser network structures and changes the permeability. While the cross-linking enhances the mechanical properties of the membrane, the permeability is generally lowered.[44,45]

The general increase of the netpoint density with a rising molar mass was already shown for the non-cross-linked chitosan membranes in Figure 4. However, for the formation of additional netpoints via a reaction of amino groups of the chitosan with the aldehyde groups of the cross-linking agent as shown in Figure 7, the DDA (degree of deacetylation) plays a more pronounced role than for the simple chitosan membrane. For the cross-linking reaction, a high DDA and therefore a high number of reactive amino groups lead to a higher netpoint density. This can be seen in Figure 8 for plots of the plateau storage modulus G_p', which is directly related to the netpoint density ν via eq 2, versus the ratio of chitosan to the cross-linker glyoxal. For cross-linked chitosan membranes, it is therefore not the molar mass that is dominating the level of the plateau modulus. The high molar mass chitosan sample (M_w = 587 kg/mol) with a DDA of 0.75 shows in a cross-linked state a lower plateau modulus than the lower molar mass sample (M_w = 318 kg/mol) that has a higher DDA of 0.79.

As expected, the amount of cross-linker correlates with the modulus as shown in Figure 8. Interestingly, the length of the cross-linker plays an important role. As one can see in Figure 8, the cross-linker glutaraldehyde leads to much smaller plateaus than glyoxal. This cannot only be explained by an increased mesh width. A possible explanation might be a lower cross-link density due to a steric hindrance of the connection of two bulky glucosamine units via the short glyoxal, whereas the longer glutaraldehyde may reduce a steric tension and therefore lead to the observed higher G_p' value.

The molar mass M_e of the polymer strands between two netpoints can roughly be estimated from the netpoint density ν (obtained from the plateau modulus (eq 2)):

$$M_e = \frac{cN_A}{\nu} \tag{7}$$

This molar mass M_e as well as the mesh width ζ_e between two netpoints

$$\zeta_e = \sqrt[3]{\frac{1}{\nu}} \tag{8}$$

have values orders of magnitude larger than the cross-linker itself. The increased netpoint density is therefore probably related to kinetic effects of the reaction; however, this needs further investigation.

The permeability of the cross-linked membranes is drastically reduced as compared to the simple chitosan membranes. As can be seen in Figure 9 for glycerol swollen membranes and different degrees of cross-linking, the relative water vapor permeability (eq 4) is reduced by nearly a factor of 2; however, the reduction seems to be nearly independent of the cross-linker concentration and is on the order of the permeability of the non-cross-linked membrane below the critical swollen state of Figure 3.

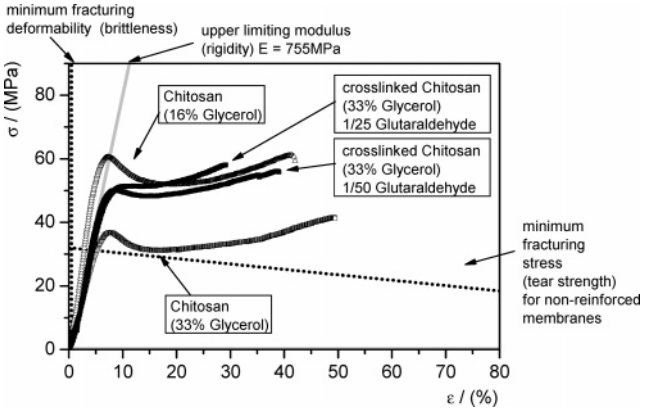

Figure 10. Stress σ as a function of the applied strain ϵ for chitosan membranes (swollen with 33 wt % glycerol) with different degrees of cross-linking. For comparison, the data for a non-cross-linked membrane, swollen with 16% glycerol, are also shown. In addition, the different critical stress and strain limits for the applicability of membranes as wet wound dressings are given.

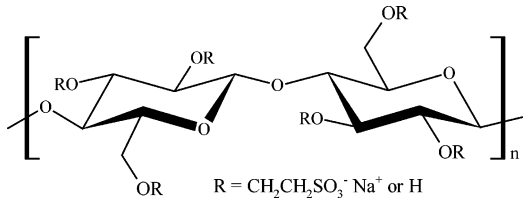

Figure 11. Structure of the anionic polymer sulfoethyl cellulose utilized for the formation of symplex membranes with chitosan.

The advantage of cross-linking the membrane is demonstrated in Figure 10 for the mechanical properties of the stress−strain experiment for a chitosan membrane containing 33% glycerol. The cross-linking seems not to change the slope of the curves and therefore does not change the Young's modulus, while at the same time the rupture stress level is remarkably increased and reaches values of the un-cross-linked chitosan membrane with only 16% glycerol, also shown in Figure 10, which already shows Young's moduli above the critical value of 755 MPa.

3.1.3. Chitosan Symplexes. A weaker linking of the partially cationic chitosan macromolecules can be achieved via the formation of a symplex (polyelectrolyte complex). The addition of polymers with oppositely charged backbone or side groups leads to electrostatic interactions of the charged polymers and the formation of a supramolecular aggregated structure (symplex) that can stabilize the membrane and accelerate the membrane formation process.[46]

However, due to the polymeric character of the counterions, the membrane properties strongly depend on the molar mass and the charge distribution along the chain of the chitosan.[47,48] During the temporal evolution of the symplex formation, a tendency for a pronounced self-acceleration of local aggregation is observed, especially for low molar masses and high ionic strength of the anionic component.[49] This may lead to the formation of isolated flakes, rather than a homogeneous membrane.

The dependence of the membrane parameters on the molecular properties of the chitosan and sulfoethyl cellulose (SEC) as the counterion (Figure 11) is investigated in the following. The investigated membranes were synthesized using a spontaneous interfacial reaction of two solutions of the charged polymers. The thickness of the formed insoluble membrane is in this case solely determined by the diffusivity of the reactants into the membrane and cannot be altered for a given polymer system.

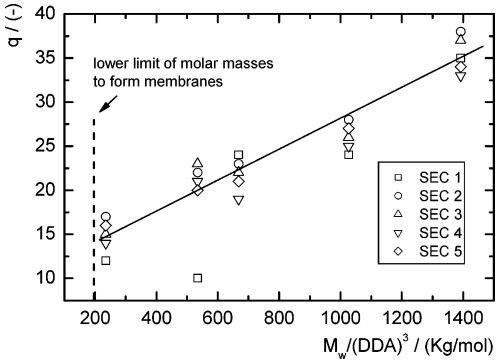

Figure 12. Swelling ratio q for different chitosan/sulfoethyl cellulose symplexes depending on the reduced molar mass $M_W/(\mathrm{DDA})^3$ of the utilized chitosan samples.

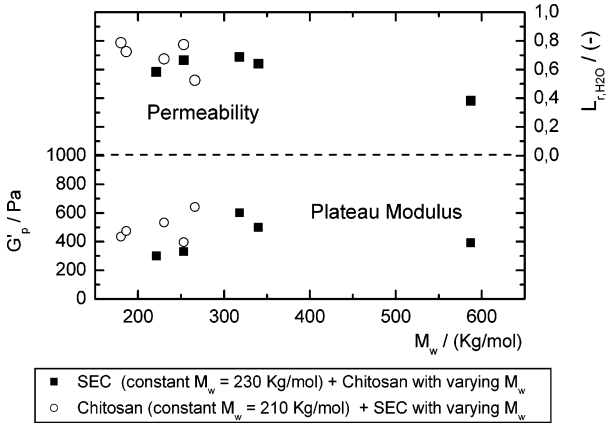

Figure 13. Plateau modulus G_p' and relative water vapor permeability L_{r,H_2O} as a function of the molar mass of the chitosan (for a constant molar mass of the sulfoethyl cellulose) or of the SEC (for a constant mass of the chitosan).

The correlation of the swellability of the membrane to molecular parameters of the chitosan/SEC symplex membranes is shown in Figure 12.

Because it is not possible to determine an exact volume for the very thin dried symplex membrane, the swelling ratio is in this case defined as the ratio q of mass of entrapped solvent to dry mass of the membrane.

$$q = \frac{m_{\mathrm{wet}} - m_{\mathrm{dry}}}{m_{\mathrm{dry}}} \tag{9}$$

The DDA (degree of deacetylation) is the second factor determining the netpoint number because less DDA and therefore less NH_3^+-ions lead to fewer possible aggregation points and therefore fewer collapsed regions and better possibilities to form a network mesh. Because the reduction of netpoints along the strain leads to expanding meshes in three dimensions, the swellability is correlated to the cubed inverse degree of deacetylation, $1/(\mathrm{DDA})^3$. Both dependencies of the swellability q are shown in Figure 12. As one can see in Figure 12, the swellability rises with an increasing molar mass and a decreasing DDA of the chitosan.

In contrast to this, the plateau moduli G_p' and hence the netpoint densities ν do not show the same trend and seem to be independent of the molar mass as can be seen in Figure 13.

The plateau moduli are relatively constant for different molar masses and therefore swellabilities, meaning that, although a rising molar mass leads to an increasing number of entanglement points in the dry state, the network swells to a nearly constant

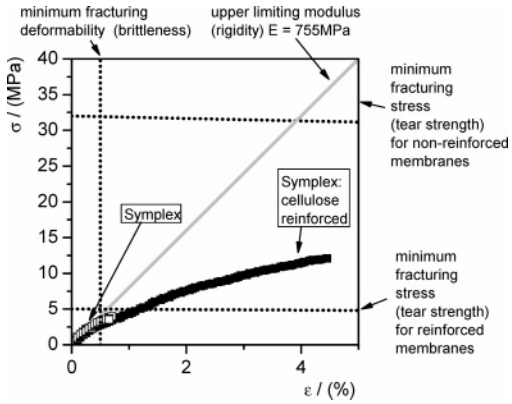

Figure 14. Stress σ as a function of the applied strain ϵ for a chitosan/sulfoethyl cellulose symplex membrane (chitosan, $M_w = 318$ kg/mol, DDA = 0.79; SEC, $M_w = 230$ kg/mol, DS = 0.4).

mesh width in the wet state. Because we are using the same dry state density, this means that for low molar mass, more of the polymer is caught in "collapsed" regions of the network, either in an amorphous phase between the meshes or in the strands of the meshes. Therefore, a high molar mass is causing more effective netpoints in the dry state but with less material in a collapsed state, the same strand length, and therefore the same mesh width. A likely explanation is that, due to high molar mass during the symplex formation, the polymer chains were less mobile, and therefore longer parts of the chain, which are not bound to the oppositely charged polymer, can form meshes of the network. The hypothesis of a constant mesh width in the wet state is supported by the permeability of the wet membranes. The gas permeability of the symplex membranes is generally on a high level, as will be demonstrated later in comparison to other different membrane types. However, a better comparison of different symplex membranes can again be achieved by the more selective relative water vapor permeability (eq 4), as was already demonstrated for the swollen chitosan membranes in Figure 5. The relative water vapor permeability is on a high level, as can also be seen in Figure 13, but seems to be independent of the molar mass in agreement with the plateau moduli.

It should be noted that, although lower molar masses lead to denser membrane structures, below a critical molar mass (as indicated in Figure 13), it is not possible to form a continuous

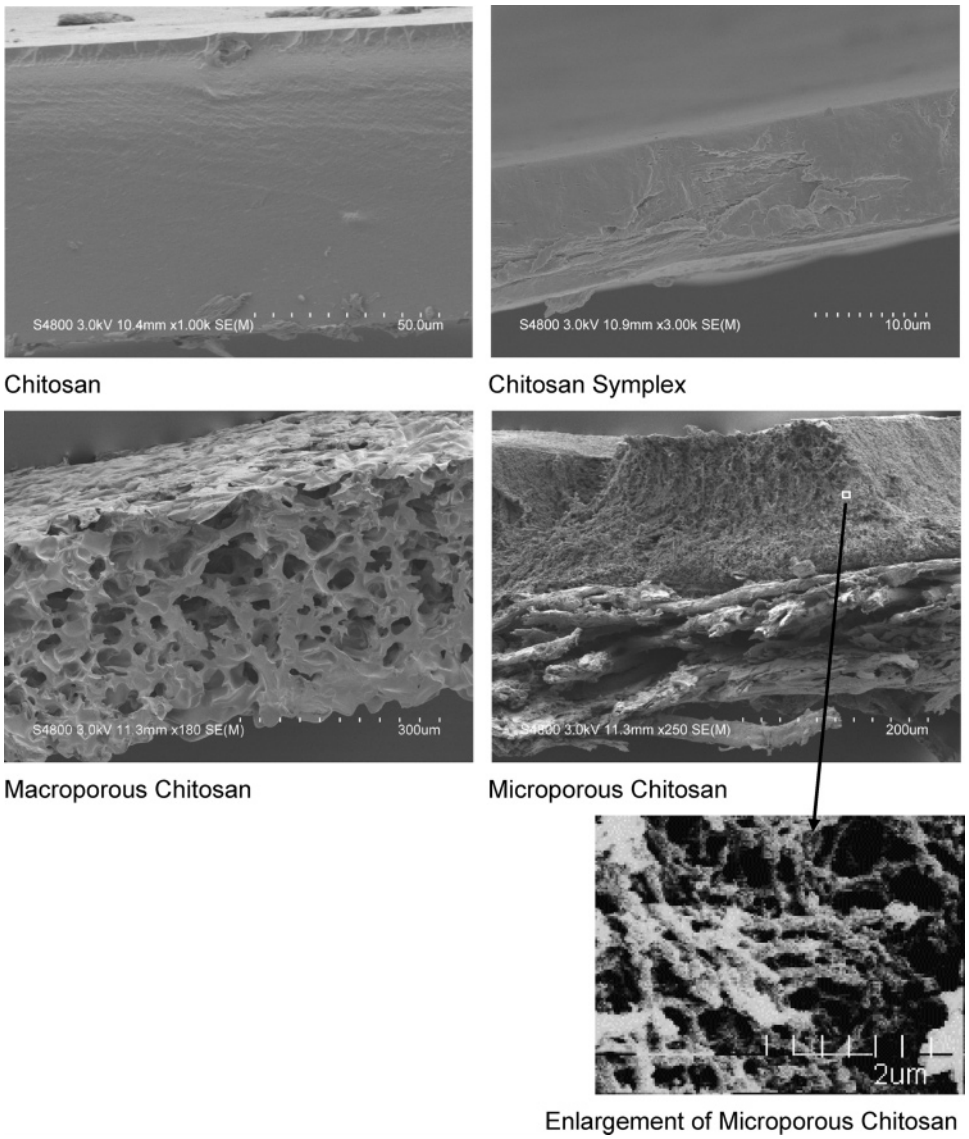

Figure 15. SEM images of different shock-frosted and freeze-dried chitosan membranes. The images are taken from crosscuts of the membranes; the microporous membrane shows in the lower half the carrier material (cellulose mesh).

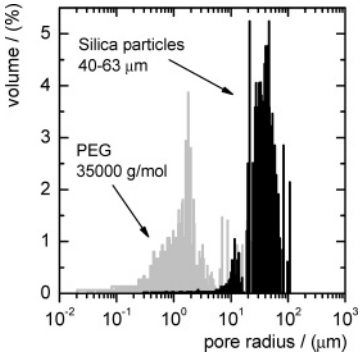

Figure 16. Volume distribution of pores in macroporous membranes (silica particles) and microporous membranes (PEG), determined from mercury porosimetry.

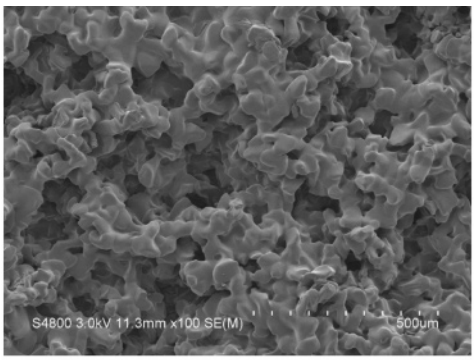

rough surface with open pores

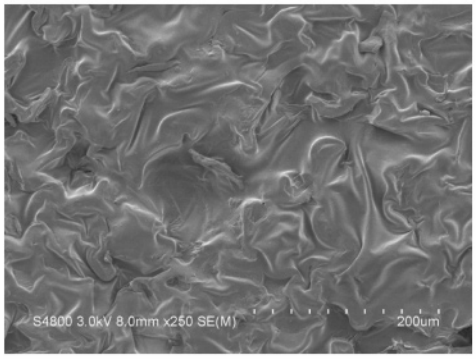

flat surface with closed pores

Figure 17. SEM images of the top and bottom surface of a shock-frosted and freeze-dried macroporous chitosan membrane, synthesized with 40−63 μm silica particles.

membrane but rather separated and dense flakes that show nearly no swellability.

In terms of varying the molar mass of the SEC, the observed swellability and plateau modulus and permeability are nearly independent of the used SEC so that it is solely the decreased charge density of the chitosan (determined by the DDA (degree of deacetylation)) that dominates the selectivity of the symplex formation process.[46]

Chitosan symplex membranes show a very low mechanical strength, as demonstrated in Figure 14, and generally have a rupture stress level much below the minimum sustainable stress level defined in the workspace diagram of Figure 6.

Because the thickness of symplex membranes cannot be adjusted due to the formation process, the only way to make symplex membranes available for application is to reinforce the structure with a carrier substrate such as a cellulose gauze, as is also shown in Figure 14. While this wide meshed material does not influence the permeability, it not only greatly improves the rupture stress level, but also increases the mechanical stability against punctual rupture. This results in the requirement to redefine the empirical critical fracture stress level of Figure 6. For reinforced membranes, this level is much lower, shown in Figure 14 as the minimum fracturing stress level for a reinforced material. Again, it should be noted that this stress level was determined purely empirical from hands-on application of the membranes to the human skin in a series of experiments in our laboratory. A comparison of this stress level to the stress−strain curve of the reinforced material shows that the reinforced symplex membrane is applicable as wound dressing.

3.1.4. Porous Chitosan Membranes. The permeability of the chitosan symplex membranes is not only for water, but generally also for gases much better than for the simple chitosan membrane. This is shown in the last paragraph of the discussion in Figure 19 by a direct comparison of the permeability of oxygen, nitrogen, and carbon dioxide.

However, the introduction of artificial pores into a chitosan membrane can increase the gas permeability by orders of magnitude and reach the level of the chitosan symplex membranes. A possible way to achieve a porous structure is the introduction of rigid silica particles[43,50] or inert polymers[51,52] during the membrane formation, which are removed from the membrane afterward.

For the characterization of a "network structure" of these membranes, the oscillatory experiment is not suitable because the dimension of these artificial pores is orders of magnitude larger than the meshes in the polymeric network. For the application of this type of membrane, the network structure of the matrix is less important for the gas transport because the main part of the gas is transported through the macropores. However, the large pore dimensions may give rise to a loss of the barrier function for microorganisms. On the other hand, the increased internal surface of the macroporous membranes enables an increased immobilization of microorganisms.

Therefore, the pore dimensions of the membrane, in which the pores are now the dominating structural factor, have to be determined by other methods to test the applicability of these membranes as a wet wound dressing. Figure 15 shows cryo-SEM images of fracture edges of the different types of chitosan membranes. While simple chitosan and the chitosan symplex show a closed structure even at the larger magnifications in Figure 15, the artificial pores in the macroporous membrane can clearly be seen. The pore sizes correlate roughly with the silica particle sizes (40−64 μm) because the particles were introduced and removed during the membrane formation in the swollen, wet state. The pore size can therefore be selected by introducing different silica particle sizes with a realistic minimum particle size of ~5 μm.[49]

Smaller pores can be introduced by replacing the silica spacers with a coiled polymer such as poly(ethylene glycol) (PEG) that can also selectively removed from the membrane after the formation.[51,52] As shown, for example, in Figure 15, for a membrane synthesized in the presence of poly(ethylene glycol) with a molar mass of 35 000 g/mol, a microporous structure can be observed. The enlargement in Figure 15 shows pores with dimensions on the order of several micrometers. The pore size distribution cannot be directly obtained as in the case of the solid silica particles of the macroporous membrane, but can be measured utilizing mercury porosimetry. Figure 16 shows a comparison of the pore size distribution for freeze-dried samples determined for the macroporous membrane with a peak average value as expected around 50 μm, and the microporous chitosan

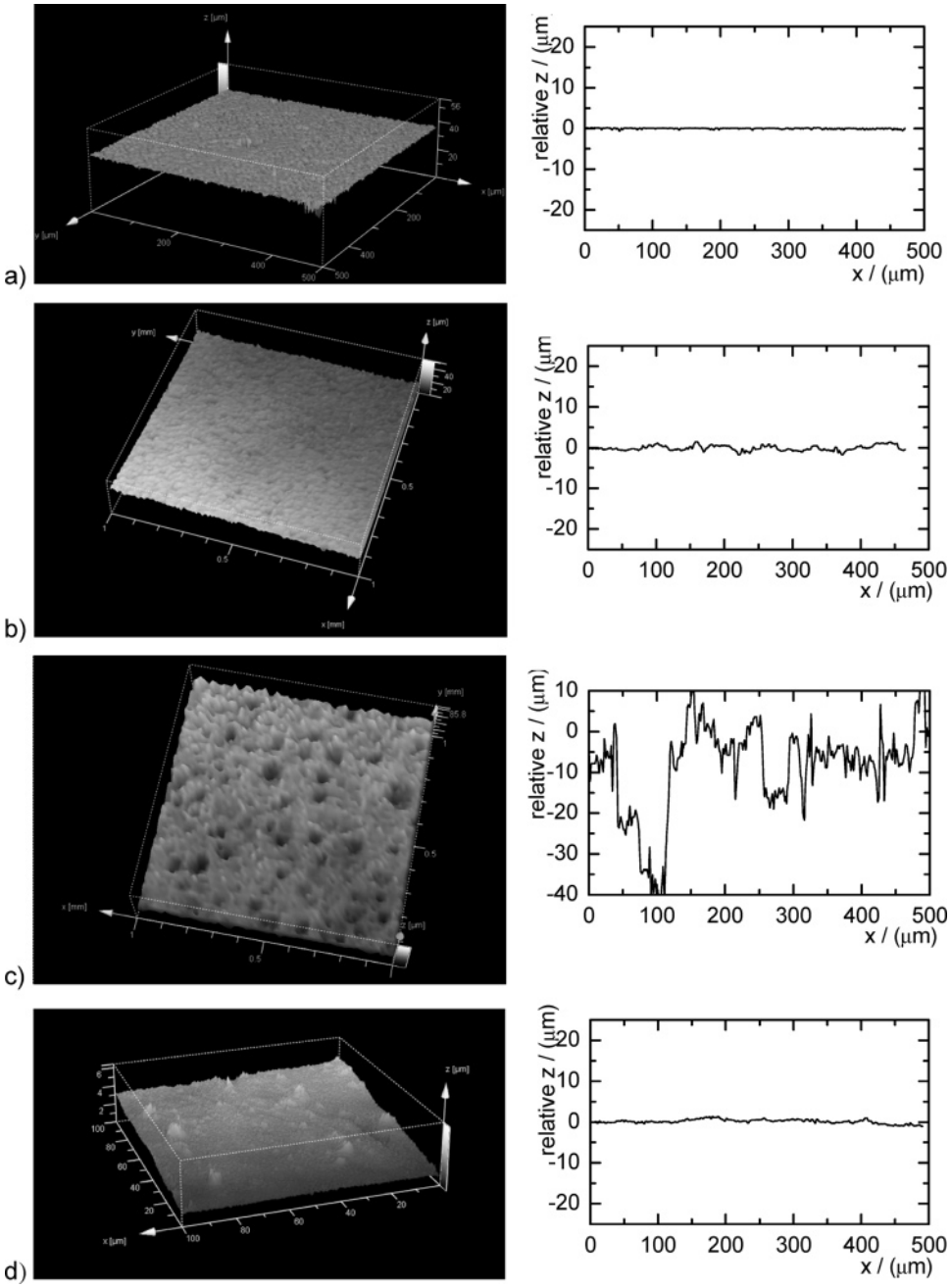

Figure 18. Left-hand side: confocal microscopy images of wet and completely swollen chitosan membranes, (a) simple chitosan membrane; (b) macroporous chitosan membranes, flat side; (c) macroporous chitosan membranes, rough side; (d) microporous membrane, rough side. Right-hand side: depth profiles of crosscuts across the membranes.

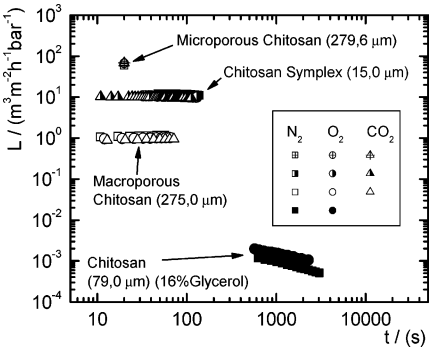

Figure 19. Gas permeability *L* for different membrane types.

membrane for which the poly(ethylene glycol) introduced a pore size distribution with a peak-average value of ~2 μm.

The barrier function of the macroporous chitosan membrane is questionable due to the large pore radii. However, the pore size distribution is not homogeneous across the membrane. Because of the method of formation on a flat carrier material, an asymmetric structure of the membrane results,[53] which was already observable in Figure 15 for the crosscut of the macroporous membrane, with a much denser structure and fewer pores at the bottom. As can be seen in Figure 17 for snapshots of the rough and the flat surface of the macroporous membrane, again obtained in the wet state with cryo-SEM, the flat side shows no open pores in comparison to the rough side. This results in a closed surface structure, similar to the simple chitosan membranes and a similar barrier function regardless of the macroporosity of the membrane body.

However, even though cryo-SEM visualization of the surface morphology gives detailed information, it cannot be ruled out

that the cryo-drying process alters the sample, especially the sensitive surface structure. A more accurate investigation of the surface morphology in a truly wet state is possible with confocal laser microscopy that allows for a quantitative analysis of the pore sizes, depth, and therefore the determination of an open or closed surface. As one can see in Figure 18a from the depth profile of a crosscut along the surface, the simple chitosan membrane has a smooth and closed surface with a roughness of $\sim 1\ \mu$m.

The flat side of the macroporous membrane, Figure 18b, shows a similar closed surface. However, due to the pores underneath, the surface is more textured, as could already be observed in the cryo-SEM pictures of Figure 17. The rough side of the macroporous membrane (c) shows, as expected, an open pore structure with indentations deeper then the correlated pore width. In contrast to this, the rough side of the microporous membrane (d) shows a much smoother surface structure.

Both micro- and macroporous membranes need a reinforcement similar to that of the chitosan symplexes to show a mechanical stability comparable to the pure chitosan membranes that is sufficient to handle and apply the membranes. Examples for stress strain experiments are given in the final part of the discussion.

3.2. Comparison of Membranes. The different types and alterations of chitosan membranes mentioned in this report all show differences in permeability and strength due to variations of the molecular parameters as molar mass, DDA (degree of deacetylation), etc., and those differences have been treated in detail in the above discussion. However, these property variations are minor as compared to differences between varying cross-linking mechanisms or different membranes. In the following, we will therefore directly compare representative membranes of the different approaches presented in this paper regarding their physical properties and their applicability as wet wound dressings.

Figure 19 gives a comparison of the gas permeability of the different types of membranes. In this case, the permeability is defined as the gas volume V per time t that permeates through an area A of membrane for a pressure gradient Δp across the membrane:

$$L = \frac{V}{tA\Delta p} \tag{10}$$

It should be noted that for each type of membrane a representative average permeability range was selected for comparison; the permeability of one type of membrane can again be adjusted in a smaller range as discussed previously by changing internal structural parameters such as network structure or pore size density. The permeabilities in Figure 19 are for membranes of different thicknesses. This representation is justified because the shown thicknesses d represent typical values for the application, obtained for the respective formation process of a membrane.

For a direct comparison of the material permeability, Figure 20 gives the reduced permeability L_{red},

$$L_{red} = Ld \tag{11}$$

which is independent of the membrane thickness and depends only on the membrane structure. Obviously, the order of magnitude thinner symplex membranes have in this respect a lower permeability, comparable to the macroporous membranes. Still, simple chitosan membranes show by far the least permeability for gases.

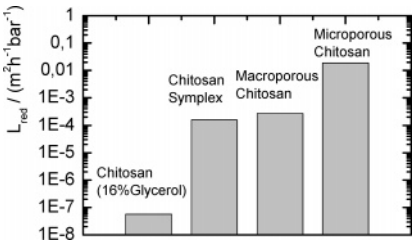

Figure 20. Reduced gas permeability L_{red} of oxygen for different membrane types.

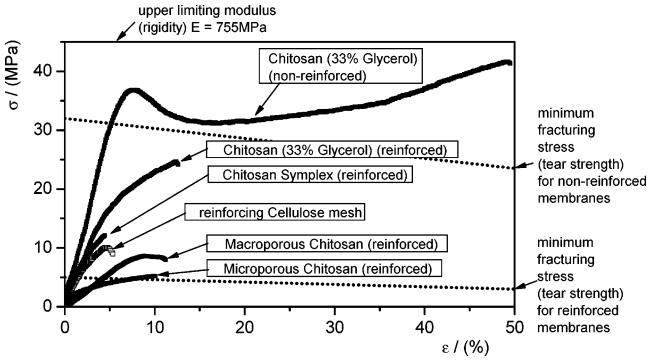

Figure 21. Stress σ as a function of the applied strain ϵ for different membrane types.

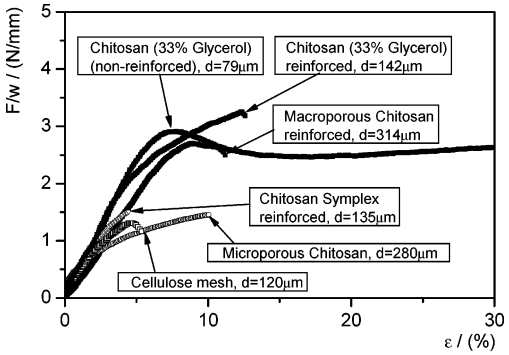

Figure 22. Force F per crosscut length w for different membrane types.

A comparison of the mechanical strength of the different membranes is given in Figure 21. It should first be noted that the stress−strain data of the weaker materials discussed previously are given in this figure for cellulose reinforced membranes, because this is the only modification that can be used in applications as wet wound dressings. The stability of nonreinforced membranes, where available, was mentioned previously. Second, the stress data are referring to the whole membrane crosscut area to directly compare the actual material strength of the membrane structures with the critical membrane parameters introduced in Figure 6 for nonreinforced and in Figure 14 for reinforced membranes.

However, this approach does not allow the separation of the stress contribution between the polymer membrane and the cellulose carrier material. For a weaker polymer membrane, this may lead to weaker reduced stresses than for the pure cellulose, as was, for example, observed for the microporous membrane in Figure 21. To give a better comparison of the mechanical strength of the different membrane types, we give in Figure 22 the force F per crosscut length w along the cellulose mesh by multiplying the stress by the membrane thickness:

$$\frac{F}{w} = \sigma d \tag{12}$$

This approach gives the mechanical strength for the typical thickness of the reinforced membrane type. However, it should be kept in mind that these values will change if the membrane thickness is altered for systems where this is possible. It can now clearly be seen that for mechanically weak polymer membrane components such as the symplex or microporous membrane, the stability is mainly controlled by the stronger reinforcing cellulose mesh. For the case of a stronger polymer component (as compared to the cellulose mesh), as, for example, the pure chitosan, Figure 22 shows that the maximum sustainable force is actually controlled by the polymer rather than the reinforcement.

4. Conclusions

The permeability and mechanical strength of chitosan membranes can be adjusted by several different methods.

The permeability of chitosan membranes can be increased by swelling of the membrane with glycerol above a critical mesh width. At the same time, the membrane becomes more flexible and loses mechanical strength. An optimum mass ratio glycerol/chitosan of ~33% results in a membrane that just meets the empirically determined Young's moduli and minimum required stresses for an application as a wound dressing.

An additional cross-linking of the chitosan with dialdehydes increases the mechanical strength while keeping the Young's modulus; however, the permeability is lowered significantly. The number density of cross-links correlates with the degree of deacetylation (DDA), whereas an increasing length of the cross-linker leads to weaker network structures.

The formation of a symplex membrane via electrostatic interaction of the chitosan with the anionic counterion sulfoethyl cellulose leads to thin and highly permeable membranes. However, the mechanical strength of symplex membranes is too low for a practical application. The symplex membrane can be reinforced by a carrier material (cellulose mesh) to increase the mechanical strength at roughly the same permeability. The reinforced membranes show a pronounced resistance against punctual rupture and require a new set of empirical critical Young's moduli and minimum stresses.

The permeability of a sufficiently strong chitosan membrane can be increased by introducing artificial pores. The introduction of inert particles or polymers during the membrane formation and the subsequent removal create macro- and microporous structures with variable pore sizes in a range of 0.5−100 μm and superior gas and fluid transport capabilities. However, these membranes need reinforcement similar to the symplex membranes to reach the required mechanical strength for an application as a wound dressing. Because of the formation conditions, an asymmetric pore size distribution and closed surface structure ensure the microbial barrier function even for the macroporous membrane structures.

A comparison of the different reinforced chitosan membrane types shows that they meet the minimum mechanical strengths required, so that the permeability can be precisely adjusted to the desired parameters of a certain wound type. For burns with a required moist wound climate but high exudate permeabilities away from the wound with at the same time good antibacterial barrier function, cross-linked macroporous membranes on a carrier material promise to be most suited as wet wound dressings. For chronic wounds with a required less moist climate but a high gas exchange to avoid anaerobe conditions, reinforced symplex membranes are the most promising candidates for tailored wet wound dressings. Ongoing clinical studies of these new membrane types have to prove their applicability.

Already the single formation techniques to modify a membrane allow for novel ways to tune and alter a membrane to show and enhance a specific material property. However, it is in particular the demonstrated possibility to join these techniques to create truly unique membranes that combines the different desired material functions in an up to now unequaled way. These membranes allow for a tailored adjustment of single parameters while at the same time the overall material properties are maintained. Parts of these novel combined membrane alterations and formation techniques are now covered by the patent DE 102004047115.

Acknowledgment. We would like to thank Prof. J. Kötz, Universität Potsdam, for conducting the SEM measurements, and Dr. S. Wessel, Beiersdorf AG Hamburg, for the confocal microscopy imaging of the membranes. We would also like to thank the Bundesministerium für Bildung und Forschung for the financial support under the project "Aerobe mikrobielle Aufarbeitung von Shrimpschalenabfällen und Produktion von Chitin als Vorstufe von Chitosan und technische Umsetzung (BMBF-05-203)", and the "Arbeitsstelle für Wissens- und Technologietransfer (AWITT)" and the Patentverwertungsagentur of the City of Hamburg for their support.

References and Notes

(1) Winter, G. D. *Nature* **1962**, *193*, 293−294.
(2) Chung, L. Y.; Schmidt, R. J.; Hamlyn, P. F.; Sagar, B. F.; Andrews, A. M.; Turner, T. D. *J. Biomed. Mater. Res.* **1994**, *28*, 463−469.
(3) Turner, T. D. *J. Sterile Serv. Man.* **1985**, *2*, 3−6.
(4) Application: DE 93-43281904328190, Water-absorbing wound dressing.
(5) Martin, P. *Science* **1997**, *276*, 75−81.
(6) Alvarez, O. M.; Patel, M.; Booker, J.; Markowitz, L. *Wounds-Compend. Clin. Res. Pract.* **2004**, *16*, 224−233.
(7) Yusof, N.; Wee, A.; Lim, L. Y.; Khor, E. *J. Biomed. Mater. Res., Part A* **2003**, *66A*, 224−232.
(8) Liang, Z. P.; Feng, Y. Q.; Meng, S. X.; Liang, Z. Y. *Chin. Chem. Lett.* **2005**, *16*, 135−138.
(9) Ma, X. L.; Yao, Z. H. *Spectrosc. Spectral Anal.* **2005**, *25*, 456−459.
(10) Azad, A. K.; Sermsintham, N.; Chandrkrachang, S.; Stevens, W. F. *J. Biomed. Mater. Res., Part B* **2004**, *69B*, 216−222.
(11) Obara, K.; Ishihara, M.; Ishizuka, T.; Fujita, M.; Ozeki, Y.; Maehara, T.; Saito, Y.; Yura, H.; Matsui, T.; Hattori, H.; Kikuchi, M.; Kurita, A. *Biomaterials* **2003**, *24*, 3437−3444.
(12) Illum, L. *Pharm. Res.* **1998**, *15*, 1326−1331.
(13) Singla, A. K.; Chawla, M. *J. Pharm. Pharmacol.* **2001**, *53*, 1047−1067.
(14) Krajewska, B. *Sep. Purif. Technol.* **2005**, *41*, 305−312.
(15) Mitra, S.; Gaur, U.; Ghosh, P. C.; Maitra, A. N. *J. Controlled Release* **2001**, *74*, 317−323.
(16) Park, P. J.; Je, J. Y.; Byun, H. G.; Moon, S. H.; Kim, S. K. *J. Microbiol. Biotechnol.* **2004**, *14*, 317−323.
(17) Liu, H.; Du, Y. M.; Wang, X. H.; Sun, L. P. *Int. J. Food Microbiol.* **2004**, *95*, 147−155.
(18) Park, S. I.; Daeschel, M. A.; Zhao, Y. *J. Food Sci.* **2004**, *69*, M215−M221.
(19) Hu, S. G.; Jou, C. H.; Yang, M. C. *Carbohydr. Polym.* **2004**, *58*, 173−179.
(20) Germany 102004047115, Verfahren zur Herstellung einer Wundauflage.
(21) Knop, S. Dissertation; University of Hamburg: Hamburg, 2000; p 161.
(22) Kulicke, W.-M.; Clasen, C. *Viscosimetry of Polymers and Polyelectrolytes*; Springer: Heidelberg, 2004.
(23) Hudson, S. M.; Smith, C. In *Biopolymers from Renewable Resources*; Kaplan, D. L., Ed.; Springer: Berlin, 1998; p 96.
(24) Li, Q.; Grandmaison, E. W.; Goosen, M. F. A.; Dunn, E. T. *J. Bioact. Compat. Polym.* **1992**, *7*, 370−397.
(25) Yang, Y. H.; Yang, H. F.; Yang, M. H.; Liu, Y. L.; Shen, G. L.; Yu, R. Q. *Anal. Chim. Acta* **2004**, *525*, 213−220.
(26) Tan, X. C.; Ll, M. J.; Cai, P. X.; Luo, L. J.; Zou, X. Y. *Anal. Biochem.* **2005**, *337*, 111−120.
(27) Drury, J. L.; Mooney, D. J. *Biomaterials* **2003**, *24*, 4337−4351.

(28) Suh, J. K. F.; Matthew, H. W. T. *Biomaterials* **2000**, *21*, 2589−2598.
(29) Kaminski, W.; Modrzejewska, Z. *Sep. Sci. Technol.* **1997**, *32*, 2659−2668.
(30) Babel, S.; Kurniawan, T. A. *J. Hazard. Mater.* **2003**, *97*, 219−243.
(31) Mukoma, P.; Jooste, B. R.; Vosloo, H. C. M. *J. Membr. Sci.* **2004**, *243*, 293−299.
(32) Kanti, P.; Srigowri, K.; Madhuri, J.; Smitha, B.; Sridhar, S. *Sep. Purif. Technol.* **2004**, *40*, 259−266.
(33) Macedo, M. A.; Silva, M. N. B.; Cestari, A. R.; Vieira, E. F. S.; Sasaki, J. M.; Goes, J. C.; Aguiar, J. A. *Physica B* **2004**, *354*, 171−173.
(34) Hu, Q. L.; Fang, Z. P.; Zhao, Y.; Xu, C. W. *Chin. J. Polym. Sci.* **2001**, *19*, 467−470.
(35) Balau, L.; Lisa, G.; Popa, M. I.; Tura, V.; Melnig, V. *Cent. Eur. J. Chem.* **2004**, *2*, 638−647.
(36) Larson, R. G. *The Structure and Rheology of Complex Fluids*; Oxford University Press: New York, 1999.
(37) Clasen, C.; Kulicke, W. M. *Prog. Polym. Sci.* **2001**, *26*, 1839−1919.
(38) Peter, M. G. *J. Macromol. Sci., Pure Appl. Chem.* **1995**, *A32*, 629−640.
(39) Marreco, P. R.; da Luz Moreira, P.; Genari, S. C.; Moraes, A. M. *J. Biomed. Mater. Res., Part B* **2004**, *71B*, 268−277.
(40) Liu, Y. L.; Su, Y. H.; Lai, J. Y. *Polymer* **2004**, *45*, 6831−6837.
(41) Liu, Y. L.; Su, Y. H.; Lee, K. R.; Lai, J. Y. *J. Membr. Sci.* **2005**, *251*, 233−238.
(42) Tsuru, K.; Shirosaki, Y.; Hayakawa, S.; Osaka, A.; Lopes, M. A.; Santos, J. D.; Fernandes, M. H. *Bioceramics, Vol. 17*; Trans Tech Publications Ltd.: Zurich-Uetikon, 2005; Vol. 17, pp 823−826.
(43) Gumusderelioglu, M.; Agi, P. *React. Funct. Polym.* **2004**, *61*, 211−220.
(44) Nakatsuka, S.; Andrady, A. L. *J. Appl. Polym. Sci.* **1992**, *44*, 17−28.
(45) Zeng, X. F.; Ruckenstein, E. *J. Membr. Sci.* **1998**, *148*, 195−205.
(46) Knop, S.; Thielking, H.; Kulicke, W. M. *J. Appl. Polym. Sci.* **2000**, *77*, 3169−3177.
(47) Wang, H. F.; Li, W. J.; Lu, Y. H.; Wang, Z. L. *J. Appl. Polym. Sci.* **1997**, *65*, 1445−1450.
(48) Dunn, E. J.; Zhang, X.; Sun, D.; Goosen, M. F. A. *J. Appl. Polym. Sci.* **1993**, *50*, 353−365.
(49) Wilhelms, T. A. Dissertation; University of Hamburg: Hamburg, 2005; p 301.
(50) Zeng, X. F.; Ruckenstein, E. *Ind. Eng. Chem. Res.* **1996**, *35*, 4169−4175.
(51) Zeng, M. F.; Fang, Z. P.; Xu, C. W. *J. Appl. Polym. Sci.* **2004**, *91*, 2840−2847.
(52) Zeng, M. F.; Fang, Z. P. *J. Membr. Sci.* **2004**, *245*, 95−102.
(53) Larena, A.; Caceres, D. A. *Appl. Surf. Sci.* **2004**, *238*, 273−277.

BM060486X